ADVANCED MATERIALS INTERFACES
www.advmatinterfaces.de

Metal–Insulator Transition Induced by Oxygen Vacancies from Electrochemical Reaction in Ionic Liquid-Gated Manganite Films

Chen Ge, Kui-Juan Jin,* Lin Gu,* Li-Cong Peng, Yong-Sheng Hu, Hai-Zhong Guo, Hong-Fei Shi, Jian-Kun Li, Jia-Ou Wang, Xiang-Xin Guo, Can Wang, Meng He, Hui-Bin Lu, and Guo-Zhen Yang*

In correlated transitional metal oxides, the coupling of charge, spin, orbital, and lattice degree of freedoms gives rise to the rich physics, including metal–insulator transition (MIT)[1] and interface related multifunctional properties.[2] The electric field control of these intriguing phenomena in transitional metal oxides has been an important theme of research in modern condensed matter physics because of its potential application in future electronic devices.[3] However, the carrier density in transitional metal oxides is exceedingly high in general, as an example of $\approx 10^{14}$ cm^{-2} for manganites and cuprates, and thus the use of conventional field-effect transistor structure in field effect control of MIT is limited by its poor ability to modulate such high carrier density due to the dielectric breakdown of dielectrics.[3] Therefore, although the benefits of utilizing transitional metal oxides as the channel materials to realize MIT by electric field effect are widely known, the development of related researches has been quite slow due to this technological challenge. Recently, several reports shed the light of utilizing novel electric double layer transistor (EDLT) structure to manipulate the electronic phase,[4–24] or even modulate superconducting phase,[4–7] in transitional metal oxides.

Dr. C. Ge, Prof. K.-J. Jin, Prof. L. Gu, L.-C. Peng, Prof. Y.-S. Hu, Dr. H.-Z. Guo, Dr. H.-F. Shi, J.-K. Li, Prof. C. Wang, M. He, Prof. H.-B. Lu, Prof. G.-Z. Yang
Beijing National Laboratory for Condensed Matter Physics
Institute of Physics
Chinese Academy of Sciences
Beijing 100190, China
E-mail: gechen@iphy.ac.cn; kjjin@iphy.ac.cn; l.gu@iphy.ac.cn
Prof. K.-J. Jin, Prof. L. Gu, Prof. G.-Z. Yang
Collaborative Innovation Center of Quantum Matter
Beijing 100190, China
Dr. J.-O. Wang
Beijing Synchrotron Radiation Facility
Institute of High Energy Physics
Chinese Academy of Sciences
Beijing 100049, China
Prof. X.-X. Guo
State Key Laboratory of High Performance Ceramics and Superfine Microstructure
Shanghai Institute of Ceramics
Chinese Academy of Sciences
Shanghai 200050, China

DOI: 10.1002/admi.201500407

It was proposed that ionic liquids (IL) used as the gated dielectric in EDLT can form a strong electric field at the interface between IL and oxides to electrostatically manipulate the high carrier density in a range of $\approx 10^{14}$–10^{15} cm^{-2}, leading to the change of the electronic phase of transitional metal oxides, while it is not achievable via field-effect transistor gated with conventional dielectric.[4–16] However, some recent reports argued that the mechanism of electronic phase change is the creation of oxygen vacancies caused by the electric field in oxides,[17–20] instead of electrostatic carrier doping. On the other hand, some other results claimed that the change of the electronic phase in correlated oxides is the result of chemical doping via an electrochemical reaction.[21–24] Despite these great efforts that have been made, the underlying mechanism of IL gating driving MIT has been a matter of debate so far. Therefore, it is of vital importance to reveal the origin of the electrical control of MIT in transitional metal oxides using IL as gate mediums.

The perovskite manganite materials are of significant interest for those who wish to control and understand MIT in correlated oxides, as well as an excellent platform for exploring how the oxygen vacancies occur and what role they play in the electronic phase transition by electrolyte gating, because of the high correlation with the valence state of manganese determined by the oxygen stoichiometry.[2,25] In this work, we focus on a typical hole-doped perovskite oxide material, $La_{0.8}Sr_{0.2}MnO_3$ (LSMO), featured with colossal magnetoresistance and phase separation.[25] First, we will present the manipulation of the electronic phase transition by using IL gating, and the realization of a resistance increase of more than four orders of magnitude in the LSMO films. Then it will be shown that the oxygen vacancies are responsible for MIT of LSMO films. Finally from a series of comparative experiments presented in this work, we conclude that these oxygen vacancies are originated by the electrochemical reaction at the interface gated by IL electrolytes, and the amount of the trace water contained in the IL plays an indispensable role in the generation of oxygen vacancies in LSMO films.

The thin films of LSMO were grown on single crystal (001) $LaAlO_3$ (LAO) substrates by pulsed laser deposition. The cross-sectional high-angle annular dark-field (HAADF) scanning transmission electron microscopy (STEM) image exhibits the LSMO/LAO sharp interface, indicating a high quality of the epitaxial heterostructure (Figure S1, Supporting Information). It was patterned into a Hall-bar structure with coplanar

ADVANCED MATERIALS INTERFACES
www.advmatinterfaces.de

Materials Views
www.MaterialsViews.com

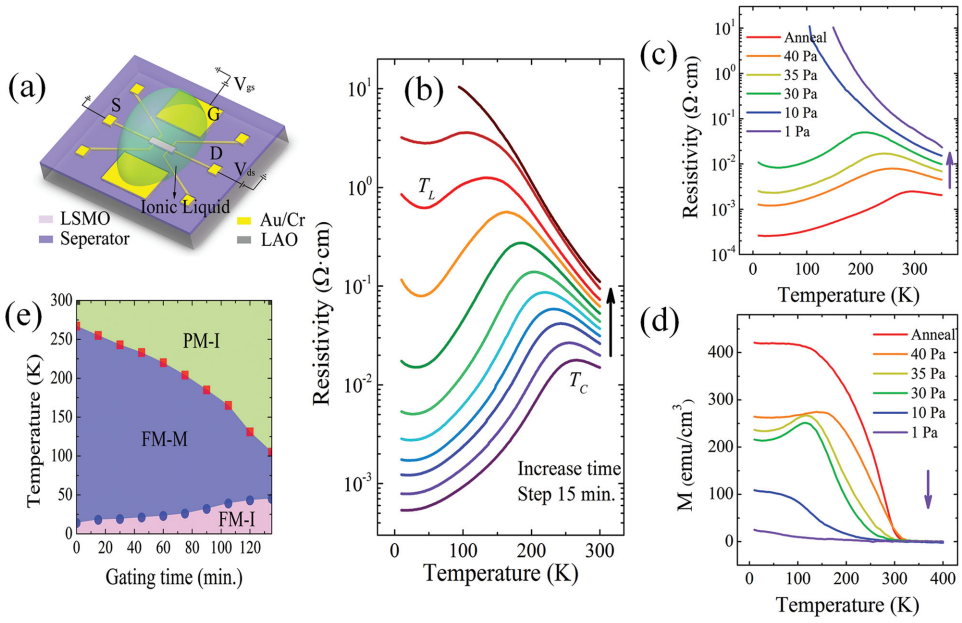

Figure 1. a) A schematic diagram of the LSMO/LAO microstructure gated with the ionic liquid, where the ionic liquid contacts the LSMO channel and the Au gate electrode. *S* presents source contact, *D* is drain contact, and *G* denotes gate electrode. b) Resistivity of LSMO versus temperature under +2.5 V gate voltage for various gating times. A fixed time step of 15 min was used, and the black arrow indicates the direction of increasing the time of applying bias. T_c and T_L denote the usual MIT temperature and low-*T* MIT temperature, respectively. c) Temperature dependence of resistivity and d) magnetization (0.1 T, field cooling) as a function of the oxygen pressure used for LSMO film deposition. The anneal sample represents that the LSMO film deposited under 40 Pa oxygen pressure was ex situ annealed in a flowing oxygen atmosphere at 600 °C for 15 min. The violet arrows denote the direction of reducing the oxygen pressures during the film growth, or the direction of increasing the amount of oxygen vacancies in manganite films. e) Phase diagram of LSMO films gated with IL under +2.5 V gate voltage for various gating times. The red squares and blue circles denote T_c and T_L extracted from (b), respectively. The abbreviations represent paramagnetic insulator (PM-I), ferromagnetic metal (FM-M), and ferromagnetic insulator (FM-I).

gates, using standard photolithography techniques. A drop of IL contacts the Hall-bar channel and the coplanar gate, schematically illustrated in **Figure 1**a (see the Experimental Section for details). The transfer curve showed a clear hysteresis loop, indicative of a nonvolatile effect (Figure S2, Supporting Information). The nonvolatile resistance remains stable during at least several weeks after washing off the IL. The bistable conductance states were achieved by applying a gate voltage of +3 V and −3 V in 15 cycles, which manifests a good reversibility (Figure S3, Supporting Information). In order to investigate the gate control of transport properties in more aspect, we measured the four-terminal resistivity as a function of temperature under +2.5 V gate voltage with various applied times (Figure 1b), in this way we can continuously manipulate the transport property. It is worth to note that the as-received IL normally contains some trace water,[22,26] which will be emphatically discussed later in this Communication. No degradation of transport property of LSMO was observed after dropping IL on devices (Figure S4, Supporting Information), demonstrating that an electrochemical reaction could be excluded under 0 V gate bias. The pristine LSMO films exhibit a metal to insulator transition at ≈270 K, which also corresponds to the ferromagnetism to paramagnetism transition.[25] The transition temperature (T_c) of LSMO films is lower than that of the bulk, which is due to the large compressive strain from the LAO substrates.[27] The black arrow in Figure 1b indicates the direction of increasing the time of applying bias. The resistivity and T_c of LSMO become larger and lower, respectively, with longer time of applying gate voltage, and eventually the LSMO channel turns to be an insulator. Interestingly, the resistivity exhibits an upturn at the low temperature and a novel insulator to metal transition emerges with the increase of the gating time. T_L, denoted as the low-temperature insulator to metal transition point, turns out to be higher with the longer time of applying gate voltage.

To understand what role oxygen vacancies play in this IL gating induced MIT, we studied both the transport and magnetic properties for LSMO films fabricated at various oxygen pressures by knowing that manganite films fabricated under lower oxygen pressure are with more oxygen vacancies.[28] The violet arrows (Figure 1c,d) exhibit the direction of reducing the oxygen pressures during the film growth, or in the other words, the direction of increasing the amount of oxygen vacancies in the manganite films. Clearly, a similar insulator to metal transition was also found at low temperature in films with more oxygen vacancies (Figure 1c). The oxygen vacancy induced large resistivity modulation of transition metal oxides is usually ascribed to the carrier doping effect[29] and the subtle lattice change.[30] Furthermore, a lower magnetic and electronic transition temperature, T_c, can also be found in manganite films fabricated under a lower oxygen pressure (Figure 1c,d) due to the suppression of the double exchange interaction by oxygen vacancies. Comparing the appearance of T_L and the lower T_c for a longer gating time (Figure 1b) with the corresponding ones in the LSMO films containing more oxygen vacancies (Figure 1c),

we can speculate that the oxygen vacancies might be responsible for the modulation of MIT in LSMO both at higher and lower temperatures (T_c and T_L), and the longer gating time might produce more oxygen vacancies. This mechanism is confirmed by our following measurements. It has been well known that the magnetism of manganites is strongly correlated with the transport properties,[25] and we also found that both the transport and magnetic properties are monotonously affected by the oxygen content in LSMO (Figure 1c,d). Thus, it can be deduced that the magnetism of LSMO gated with IL could also be modulated by applying gate voltage, and actually the control of magnetism of LSMO has been demonstrated via IL gating recently.[19] The shifts of T_c and T_L through gating under +2.5 V for various applied times are summarized in Figure 1e. We can see the ferromagnetic insulating phase (FM-I) emerging at the low temperature, in addition to the general ferromagnetic metallic phase (FM-M) and paramagnetic insulating phase (PM-I). The low temperature FM-I phase can be ascribed to the decrease of the effective doping density due to the oxygen vacancies, according to the fact that the FM-I phase emerges for $0.1<x<0.17$ in $La_{1-x}Sr_xMnO_3$.[25] From Figure 1e, we can also see that FM-M phase exists in a shorter temperature range for LSMO after longer gating time with IL. This phase diagram also strongly implies that longer gating time may correspond to more oxygen vacancies, as the oxygen vacancies can reduce the transport ability in hole-doped LSMO.

To investigate the possible underlying mechanism of the intriguing gating phenomena in the LSMO films, oxygen vacancy formation during the electrolyte gating is firstly and directly confirmed by the aberration-corrected annular-bright-field (ABF) imaging technique. Since the contrast of ABF micrograph is proportional to $Z^{1/3}$ with respect to the atomic number and is very sensitive to the light elements, it is a very promising technique to probe oxygen[28] and even lithium[31] atoms at atomic scale. Thanks to the nonvolatile nature of electrolyte gating, we can detect atomic information of the LSMO microstructures via STEM technique after applying the gate voltage and washing off IL with isopropyl alcohol. **Figure 2**a,b displays the HAADF and the corresponding ABF images of the LSMO/LAO samples after applying +2.5 V gate voltage for 90 min, respectively. The La/Sr sites are represented by the lightest spots and O sites are the darkest spots in the HADDF image, while the La/Sr sites are represented by the darkest spots and O sites are the lightest spots in the ABF image. Figure 2c–e exhibits the line profiles along the Mn-O-Mn chains marked by the black, blue, and red bars in Figure 2b, which denote the regions at the surface, in the middle, and at the LSMO/LAO interface in LSMO films, respectively. The oxygen and manganese sites are indicated by the magenta and green circles in Figure 2c–e, respectively. The shallower valley of the oxygen sites in the line profiles of Figure 2c–e represents more oxygen vacancies. It can be seen that there are sufficient oxygen atoms at the interface between films and substrates, and more and more oxygen vacancies appear along the direction from the interface of LSMO/LAO to the surface of the LSMO film. An oxygen vacancy concentration distribution along the *c*-axis direction can be found in the gated LSMO films. The depth of oxygen vacancies induced by IL gating reached a dozen of nanometers from the surface of the

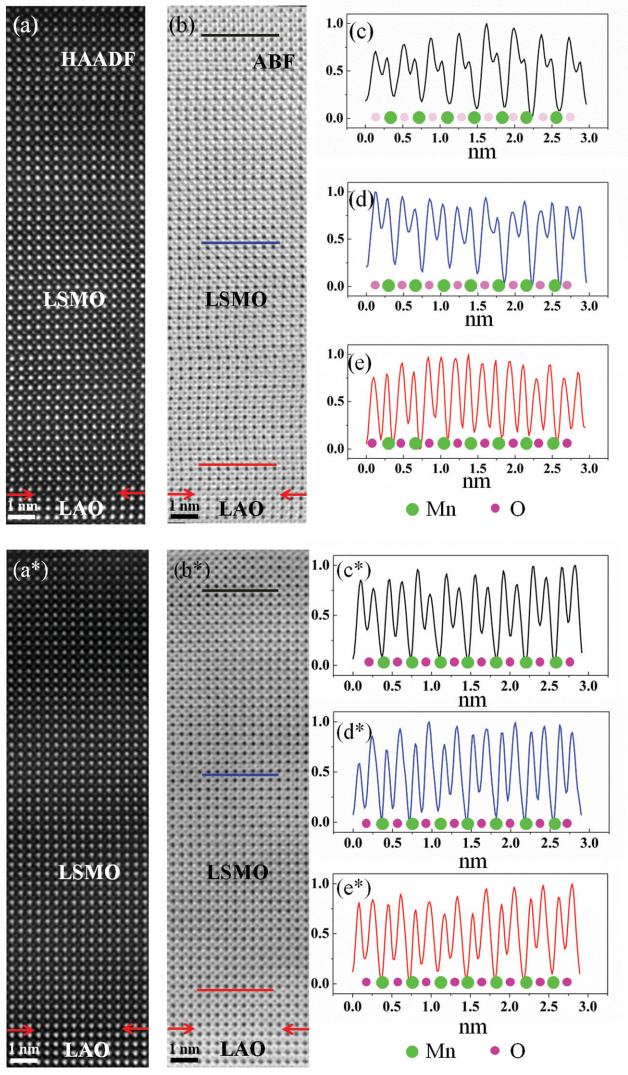

Figure 2. a) HAADF and b) ABF micrographs of LSMO/LAO heterostructures after applying +2.5 V gate voltage for 90 min. The red arrows indicate where the interface locates. c–e) Line profiles of the MnO*x* layers with respect to the black, blue, and red bars indicated in (b), respectively. The magenta/green circles display the O and Mn sites, respectively. The lighter magenta ones denote the presence of more oxygen vacancies. The asterisk (a*–e*) represents the pristine LSMO/LAO sample.

LSMO film under such conditions. For comparison, we found that oxygen vacancies almost do not exist in the whole region of the LSMO channel without gating (Figure 2a*–e*). In addition, the more pronounced shoulder peak at ≈640.0 eV and the shift of the Mn L_3 peak toward a lower energy corresponding to the appearance of a lower valence state of manganese in the Mn *L*-edge X-ray absorption spectroscopy (XAS) measurements also strongly support the presence of the oxygen vacancies in the gated LSMO, consistent with these ABF-STEM characterization results (Figure S5, Supporting Information). Therefore, the emergence of oxygen vacancies at the surface of the LSMO film implies that oxygen vacancies are produced at the interface between IL and oxides, which could be due to the extremely high electric field or the electrochemical reaction.

ADVANCED MATERIALS INTERFACES
www.advmatinterfaces.de

Materials Views
www.MaterialsViews.com

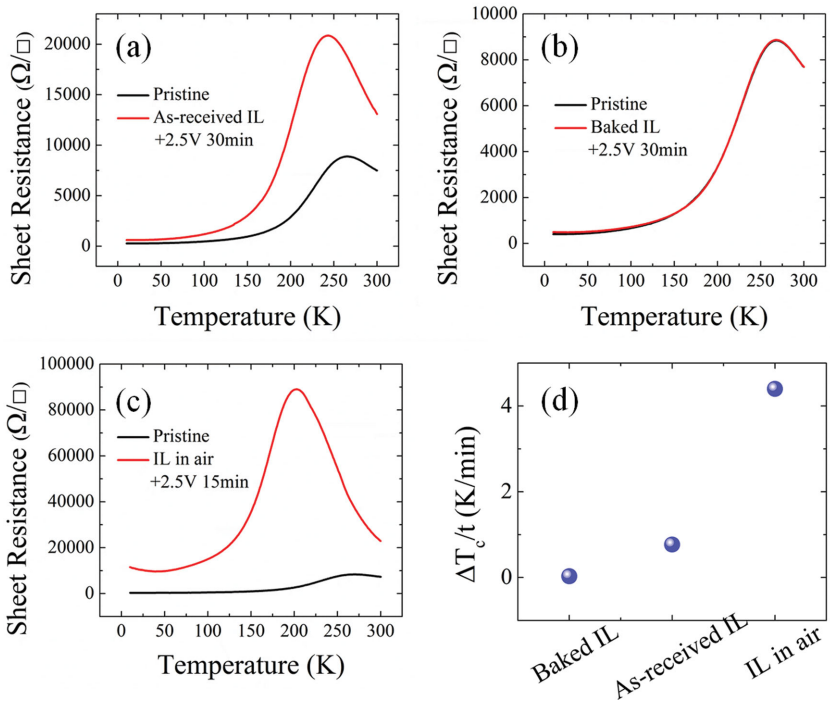

Figure 3. Gate tuned temperature dependence of sheet resistance on the a) as-received IL, b) baked IL, and c) IL exposed in air gated devices. The black lines represent *R–T* curves of the pristine LSMO, while the red lines denote *R–T* curves of the LSMO after electrolyte gating. d) The electrolyte dependence of $\Delta T_c/t$ in LSMO devices. Here, $\Delta T_c/t$ is defined as the change of the MIT temperature divided by time.

In order to reveal the origin of the generation of oxygen vacancies at the interface between IL and LSMO, we carried out a series of comparative measurements. As we have mentioned, the above measurements were all performed using the as-received IL. The IL commonly contains trace water in its fabrication process.[22,26] We found that the trace water in the as-received IL is an important factor which profoundly affects the gating experiments. Therefore, one film sample with 10 mm × 10 mm was patterned into four Hall-bar structures and then sectioned into four pieces with 5 mm × 5 mm. One device was gated with the as-received IL. The resistivity versus temperature (*R–T*) curves of the pristine LSMO and that after electrolyte gating were plotted in **Figure 3**a. The change of T_c (ΔT_c) was 23 K after applying +2.5 V bias for 30 min. The ability of generating oxygen vacancies for the electrolyte, defined as the modulation rate ($\Delta T_c/t$), is 0.77 K min^{-1} obtained from as-received IL, with t denoting the time of applying gate voltage. To remove the trace water in IL, we baked the as-received IL and the Hall-bar structure in a vacuum tube furnace (20 mTorr) at 120 °C for several days.[17] We found that the gating control of transport properties in LSMO was greatly suppressed (Figure 3b). The modulation rate is only 0.03 K min^{-1}, one order of magnitude less than that from the as-received IL. Some previous investigations have shown that the water can be easily dissolved in IL if it is exposed to ambient air.[22,32] Thus, the baked IL was exposed in ambient air for 3 d. Then, we performed the gating experiment with the exposed IL, and the data are shown in Figure 3c. The modulation rate is 4.4 K min^{-1}, more than five times larger than that with the as-received IL. The dramatically different gating phenomena strongly support that the water contaminated in IL plays a crucial role in the gating experiments. As all the modulation rates summarized in Figure 3d, larger modulation rate can be obtained with IL containing more water, while almost none obtained with baked IL (without water). As we have demonstrated from the comparison of ΔT_c in Figure 1b,c, the modulation rate corresponding to the amount of oxygen vacancies, we can conclude that more oxygen vacancies could be generated by using IL containing more water. In order to further prove this issue, the water contents in the baked, as-received, and exposed IL were measured using Karl-Fischer titration, and were found to be 92.7, 349.8, and 671.5 ppm in a 0.2 mL sample of the IL, respectively. Based on these measurements, we conclude that the amount of water inside IL plays an indispensable role in the gating control of MIT in perovskite oxides, as the source in the generation of oxygen vacancies in the electrochemical reactions between water and manganite films. The generation of oxygen vacancies by water and LSMO can be described by the following equations[33]

$$\begin{aligned} &La_{0.8}Sr_{0.2}\left[Mn^{3+}_{0.8}Mn^{4+}_{0.2}\right]O_3 + 2\delta e^- + \delta H_2O \\ &\leftrightarrow La_{0.8}Sr_{0.2}\left[Mn^{2+}_{x}Mn^{3+}_{2\delta-x};Mn^{3+}_{0.8-x}Mn^{4+}_{0.2-(2\delta-x)}\right] \\ &O_{3-\delta} + 2\delta OH^- \end{aligned} \quad (1)$$

Based on the above measurements, we schematically illustrate the process of MIT in LSMO gated with IL (**Figure 4**a–c). The pristine LSMO films exhibit a common metal to insulator transition at $T_c \approx 270$ K, with the increase of the temperature as shown in Figure 4d. Under gating bias, the LSMO films can react with the water inside IL at the interface between manganite films and IL (Equation (1)). This electrochemical reaction leads to the generation of oxygen vacancies in LSMO films and the reduction of some valence states in the manganese. ABF-STEM images confirmed that an oxygen vacancy concentration distribution along the *c*-axis direction appeared in the gated LSMO films. More oxygen vacancies emerged at the surface of the LSMO film than those at the interface of LSMO/LAO (Figure 4b). Consequently, the resistance of LSMO films increases, and T_c decreases with increasing the gating time (Figure 4e), or in other words with increasing the amount of oxygen vacancies. Eventually, the LSMO film turns to be an insulator in the entire temperature range measured (Figure 4f), when the oxygen vacancies are more enough to turn LSMO into an insulator with enough gating time. From the pristine condition, the channel resistance nearly

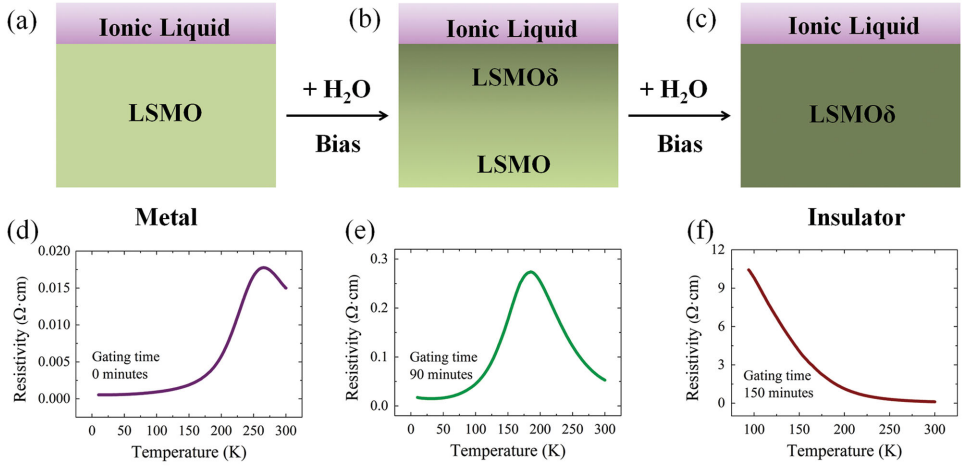

Figure 4. a–c) Schematic of the MIT in LSMO films gated with ionic liquids by applying the gate bias. LSMOδ represents the LSMO film containing oxygen vacancies. d,e,f) Resistivity versus temperature for gating times of 0, 90, and 150 min, respectively (adapted from Figure 1b).

keeps constant and the transport property almost can not be modulated after applying up to –4 V negative bias, probably because of the absence of oxygen vacancies in the pristine film (Equation (1).

The present work combined with the recent studies indicates that there may be several mechanisms behind the electronic phase modulation related to electrolyte gating in oxides. Which one dominates in these phenomena possibly depends on both the treatment of electrolyte and the choice of gated materials. There are actually electrochemical reactions using water contaminated IL as gating electrolyte, and more oxygen vacancies can be produced with more water in IL. This electrochemical mechanism can be greatly suppressed by exploiting dry IL. Nevertheless, the strong electric field at the interface between IL and oxides almost cannot induce oxygen vacancies in LSMO, different to the case in VO_2.[17] It has been reported that the resistance switching, i.e., On/Off ratio, using $LaMnO_3$ films deposited at a high oxygen pressure (10 Pa) is only 1.8 under a large voltage (5.0 V),[28] while the On/Off ratio of VO_2 can reach more than two orders of magnitude.[34] Because the migration of oxygen vacancies in transition metal oxides has been widely accepted as the origin of the resistance switching,[35,36] this difference has strongly indicated that the oxygen vacancies can much more readily migrate under an electric field in VO_2 than in $LaMnO_3$. Therefore, the mechanism that the electric field induces the migration of oxygen vacancies does not govern in MIT of LSMO devices.

In conclusion, our work demonstrates that the electronic phase of manganite films was successfully manipulated by the interfacial electrochemistry route using IL gating. The transition temperature of the usual metal to insulator transition in LSMO films becomes lower with longer gating time, and a novel insulator to metal transition in LSMO films could be achieved at low temperature after applying a small gate voltage. A resistance increase of more than four orders of magnitude and a phase diagram with gating time for LSMO films have been obtained. FM-M phase exists in a shorter temperature range for LSMO after longer gating time with as-received IL. We firstly and directly confirm the emergence of oxygen vacancies in manganite films after electrolyte gating by ABF-STEM at atomic scale and XAS measurements. The combination of comparative experiments performed in this work reveals that the oxygen vacancies are induced by the electrochemical reaction between the trace water in IL and manganites. It has also been concluded that more oxygen vacancies can be produced with longer gating time for LSMO films with IL containing water, and the slight amount of water in IL can profoundly affect the gating control of the physical properties of perovskite oxides.

Moreover, oxygen vacancies are important functional ion defects in transition metal oxides.[37] A small variation in the oxygen content can lead to the change of the valence state of the transition metal cations, which can dramatically modify the physical properties[37] The present work opens a new pathway for dynamically controlling oxygen vacancies via the electrochemical method. The possibility to manipulate oxygen vacancies also offers an opportunity toward controlling magnetism, ferroelectricity, and superconductivity of transition metal oxides in terms of electrochemistry. By understanding this mechanism behind MIT in perovskite oxides gated with IL, we can further manipulate the physical properties and utilize some functionabilities by focusing on the electrochemical reaction at the interface between IL and oxides.

Experimental Section

Thin-Film Growth: Epitaxial thin LSMO films with a thickness of 20 nm were grown on (001) $LaAlO_3$ substrates (MTI Ltd.) by pulsed laser deposition technique using a XeCl excimer laser with a laser fluence of ≈2 J cm^{-2} and a repetition rate of 2 Hz. The growth was carried out under various oxygen partial pressures at 590 °Cand the growth rate was ≈2.75 nm min^{-1}. The films for Hall-bar devices were grown under 40 Pa oxygen pressure.

Device Fabrication: The thin films were patterned into a Hall-bar channel with a coplanar gate structure by standard photolithography and argon-ion etching techniques. The channel dimension is 500 μm × 50 μm. An adhesion layer of 5 nm thick Cr was used followed by a 75 nm Au to form electrical contacts via thermal evaporation. An overlayer of a hard-baked photoresist was used as a protection layer to electrically isolate gate from channel. The device fabrication was completed by

putting a droplet of an ionic liquid *N,N*-diethyl-*N*-(2-methoxyethyl)-*N*-methylammonium bis-(trifluoromethylsulphonyl)-imide (DEME-TFSI, Kanto Chemical Co.) on the channel and side gate. Then, the device was immediately put into the PPMS vacuum chamber (Quantum Design Ltd.), and the entire exposure time in the air was less than 5 min.

Electrical Measurements: All the transfer characteristics and transport properties of the LSMO thin films and devices were measured with the Keithley 6517B Electrometer and 2400 SourceMeter in PPMS (Quantum Design Ltd.). Due to the nonvolatile nature of channel resistance by IL gating, the transport property with a standard four-probe configuration after maintaining the gate voltage for a period of time was measured. Temperature was swept from 300 to 10 K at a cooling rate of 3 K min^{-1}.

Microstructure Characterization: The samples for STEM were prepared with the Hall-bar devices in a focused ion beam scanning electron microscopy (FIB-SEM, Helios 600i). An aberration-corrected STEM JEM ARM200F (JEOL, Tokyo, Japan) provided a direct interpretation of the atomic structure at subangstrom resolution. ABF and HAADF were performed in the specimen of LSMO/LAO from the surface to interface, directly confirming the content of oxygen vacancies which play a dominant role in the variation of resistance. The collection semiangle of the ABF-STEM and HAADF-STEM detectors is 12–24 mrad and 70–250 mrad, respectively. XAS was performed via total electron yield method on the 4B9B beamline of the Beijing Synchrotron Radiation Facility (BSRF) at the Institute of High Energy Physics, Chinese Academy of Sciences, and the background vacuum level was 6×10^{-7} Torr.

Supporting Information

Supporting Information is available from the Wiley Online Library or from the author.

Acknowledgements

The authors thank K. Jin and H. Li for helpful discussion. The authors would like to thank 4B9B beam line of the Beijing Synchrotron Radiation Facility (BSRF) for XAS measurements. This work was supported by the National Basic Research Program of China (Grant No. 2014CB921001), the National Hi-tech (R&D) project of China (Grant No. 2014AA032607), and the National Natural Science Foundation of China (Grant Nos. 11134012, 11404380, 11474349, and 51222210), and the Strategic Priority Research Program (B) of the Chinese Academy of Sciences (Grant No. XDB07030200).

Received: July 27, 2015
Revised: August 13, 2015
Published online:

[1] M. Imada, A. Fujimori, Y. Tokura, *Rev. Mod. Phys.* **1998**, *70*, 1039.
[2] J. Chakhalian, J. W. Freeland, A. J. Millis, C. Panagopoulos, J. M. Rondinelli, *Rev. Mod. Phys.* **2014**, *86*, 1189.
[3] C. Ahn, A. Bhattacharya, M. Di Ventra, J. Eckstein, C. D. Frisbie, M. Gershenson, A. Goldman, I. Inoue, J. Mannhart, A. J. Millis, *Rev. Mod. Phys.* **2006**, *78*, 1185.
[4] K. Ueno, S. Nakamura, H. Shimotani, A. Ohtomo, N. Kimura, T. Nojima, H. Aoki, Y. Iwasa, M. Kawasaki, *Nat. Mater.* **2008**, *7*, 855.
[5] A. S. Dhoot, S. C. Wimbush, T. Benseman, J. L. MacManus-Driscoll, J. Cooper, R. H. Friend, *Adv. Mater.* **2010**, *22*, 2529.
[6] A. T. Bollinger, G. Dubuis, J. Yoon, D. Pavuna, J. Misewich, I. Božović, *Nature* **2011**, *472*, 458.
[7] X. Leng, J. Garcia-Barriocanal, B. Yang, Y. Lee, J. Kinney, A. Goldman, *Phys. Rev. Lett.* **2012**, *108*, 067004.
[8] A. S. Dhoot, C. Israel, X. Moya, N. D. Mathur, R. H. Friend, *Phys. Rev. Lett.* **2009**, *102*, 136402.
[9] Y. Yamada, K. Ueno, T. Fukumura, H. Yuan, H. Shimotani, Y. Iwasa, L. Gu, S. Tsukimoto, Y. Ikuhara, M. Kawasaki, *Science* **2011**, *332*, 1065.
[10] M. Nakano, K. Shibuya, D. Okuyama, T. Hatano, S. Ono, M. Kawasaki, Y. Iwasa, Y. Tokura, *Nature* **2012**, *487*, 459.
[11] R. Scherwitzl, P. Zubko, I. G. Lezama, S. Ono, A. F. Morpurgo, G. Catalan, J. M. Triscone, *Adv. Mater.* **2010**, *22*, 5517.
[12] P. H. Xiang, S. Asanuma, H. Yamada, I. H. Inoue, H. Sato, H. Akoh, A. Sawa, K. Ueno, H. Yuan, H. Shimotani, *Adv. Mater.* **2011**, *23*, 5822.
[13] P. H. Xiang, S. Asanuma, H. Yamada, H. Sato, I. H. Inoue, H. Akoh, A. Sawa, M. Kawasaki, Y. Iwasa, *Adv. Mater.* **2013**, *25*, 2158.
[14] J. Lourembam, J. Wu, J. Ding, W. Lin, T. Wu, *Phys. Rev. B* **2014**, *89*, 014425.
[15] W. N. Lin, J. F. Ding, S. X. Wu, Y. F. Li, J. Lourembam, S. Shannigrahi, S. J. Wang, T. Wu, *Adv. Mater. Interfaces* **2014**, *1*, 1300001.
[16] T. Hatano, Z. Sheng, M. Nakamura, M. Nakano, M. Kawasaki, Y. Iwasa, Y. Tokura, *Adv. Mater.* **2014**, *26*, 2874.
[17] J. Jeong, N. Aetukuri, T. Graf, T. D. Schladt, M. G. Samant, S. S. Parkin, *Science* **2013**, *339*, 1402.
[18] M. Li, W. Han, X. Jiang, J. Jeong, M. G. Samant, S. S. Parkin, *Nano Lett.* **2013**, *13*, 4675.
[19] B. Cui, C. Song, G. Wang, Y. Yan, J. Peng, J. Miao, H. Mao, F. Li, C. Chen, F. Zeng, *Adv. Funct. Mater.* **2014**, *24*, 7233.
[20] K. Fujiwara, T. Ichimura, H. Tanaka, *Adv. Mater. Interfaces* **2014**, *1*, 1300108.
[21] H. Yuan, H. Shimotani, A. Tsukazaki, A. Ohtomo, M. Kawasaki, Y. Iwasa, *J. Am. Chem. Soc.* **2010**, *132*, 6672.
[22] H. Ji, J. Wei, D. Natelson, *Nano Lett.* **2012**, *12*, 2988.
[23] A. C. Lang, J. D. Sloppy, H. Ghassemi, R. C. Devlin, R. J. Sichel-Tissot, J.-C. Idrobo, S. J. May, M. L. Taheri, *ACS Appl. Mater. Interfaces* **2014**, *6*, 17018.
[24] J. Shi, S. Ha, Y. Zhou, F. Schoofs, S. Ramanathan, *Nat. Commun.* **2013**, *4*, 2672.
[25] Y. Tokura, *Rep. Prog. Phys.* **2006**, *69*, 797.
[26] T. Sato, G. Masuda, K. Takagi, *Electrochim. Acta* **2004**, *49*, 3603.
[27] P. Dey, T. Nath, A. Taraphder, *Appl. Phys. Lett.* **2007**, *91*, 012511.
[28] Z. T. Xu, K. J. Jin, L. Gu, Y. L. Jin, C. Ge, C. Wang, H. Z. Guo, H. B. Lu, R. Q. Zhao, G. Z. Yang, *Small* **2012**, *8*, 1279.
[29] C. Schlueter, P. Orgiani, T. L. Lee, A. Y. Petrov, A. Galdi, B. A. Davidson, J. Zegenhagen, C. Aruta, *Phys. Rev. B* **2012**, *86*, 155102.
[30] R. Jaramillo, S. D. Ha, D. M. Silevitch, S. Ramanathan, *Nat. Phys.* **2014**, *10*, 304.
[31] L. Gu, C. Zhu, H. Li, Y. Yu, C. Li, S. Tsukimoto, J. Maier, Y. Ikuhara, *J. Am. Chem. Soc.* **2011**, *133*, 4661.
[32] C. D. Tran, S. H. De Paoli Lacerda, D. Oliveira, *Appl. Spectrosc.* **2003**, *57*, 152.
[33] J. T. Mefford, W. G. Hardin, S. Dai, K. P. Johnston, K. J. Stevenson, *Nat. Mater.* **2014**, *13*, 726.
[34] M. J. Lee, Y. Park, D. S. Suh, E. H. Lee, S. Seo, D. C. Kim, R. Jung, B. S. Kang, S. E. Ahn, C. B. Lee, *Adv. Mater.* **2007**, *19*, 3919.
[35] R. Waser, M. Aono, *Nat. Mater.* **2007**, *6*, 833.
[36] A. Sawa, *Mater. Today* **2008**, *11*, 28.
[37] S. V. Kalinin, N. A. Spaldin, *Science* **2013**, *341*, 858.